High efficiency single dopant white electrophosphorescent light emitting diodes

Adamovich, Vadim
Department of Chemistry, University of Southern California

Brooks, Jason
Department of Chemistry, University of Southern California

Tamayo, Arnold
Department of Chemistry, University of Southern California

Alexander, Alex M.
Department of Chemistry, University of Southern California

他

http://hdl.handle.net/2324/19451

High efficiency single dopant white electrophosphorescent light emitting diodes†

Vadim Adamovich,[a] Jason Brooks,[a] Arnold Tamayo,[a] Alex M. Alexander,[a] Peter I. Djurovich,[a] Brian W. D'Andrade,[b] Chihaya Adachi,[c] Stephen R. Forrest*[b] and Mark E. Thompson*[a]

[a] Department of Chemistry, University of Southern California, Los Angeles, CA 90089, USA.
  E-mail: met@usc.edu
[b] Center for Photonics and Optoelectronic Materials (POEM), Princeton Materials Institute (PMI),
  Department of Electrical Engineering, Princeton University, Princeton, NJ 08544, USA.
  E-mail: forrest@princeton.edu
[c] Department of Photonics Materials Science, Chitose Institute of Science & Technology, 758-65 Bibi,
  Chitose 066-8655, Japan

Efficient white electrophosphorescence has been achieved with a single emissive dopant. The dopant in these white organic light emitting diodes (WOLEDs) emits simultaneously from monomer and aggregate states, leading to a broad spectrum and high quality white emission. The dopant molecules are based on a series of platinum(II) [2-(4,6-difluorophenyl)pyridinato-$N,C^{2'}$] β-diketonates. All of the dopant complexes described herein have identical photophysics in dilute solution with structured blue monomer emission (λ_{max} = 468, 500, 540 nm). A broad orange aggregate emission ($\lambda_{max} \approx 580$ nm) is also observed, when doped into OLED host materials. The intensity of the orange band increases relative to the blue monomer emission, as the doping level is increased. The ratio of monomer to aggregate emission can be controlled by the doping concentration, the degree of steric bulk on the dopant and by the choice of the host material. A doping concentration for which the monomer and excimer bands are approximately equal gives an emission spectrum closest to standard white illumination sources. WOLEDs have been fabricated with doped CBP and mCP luminescent layers (CBP = N,N'-dicarbazolyl-4,4'-biphenyl, mCP = N,N'-dicarbazolyl-3,5-benzene). The best efficiencies and color stabilities were achieved when an electron/exciton blocking layer (EBL) is inserted into the structure, between the hole transporting layer and doped CBP or mCP layer. The material used for an EBL in these devices was *fac*-tris(1-phenylpyrazolato-$N,C^{2'}$)iridium(III). The EBL material effectively prevents electrons and excitons from passing through the emissive layer into the hole transporting NPD layer. CBP based devices gave a peak external quantum efficiency of $3.3 \pm 0.3\%$ (7.3 ± 0.7 lm W^{-1}) at 1 cd m^{-2}, and $2.3 \pm 0.2\%$ (5.2 ± 0.3 lm W^{-1}) at 500 cd m^{-2}. mCP based devices gave a peak external quantum efficiency of 6.4% (12.2 lm W^{-1}, 17.0 cd A^{-1}), CIE coordinates of 0.36, 0.44 and a CRI of 67 at 1 cd m^{-2} (CIE = Commission Internationale de l'Eclairage, CRI = color rendering index). The efficiency of the mCP based device drops to $4.3 \pm 0.5\%$ (8.1 ± 0.6 lm W^{-1}, 11.3 cd A^{-1}) at 500 cd m^{-2}, however, the CIE coordinates and CRI remain unchanged.

The efficiencies and color purities of monochromatic organic light emitting diodes (OLEDs) have improved markedly over the last five years, leading to devices with close to 100% internal quantum efficiencies.[1] While the progress toward achieving high efficiency in white OLEDs (WOLEDs) has been slower, there have nonetheless been significant advances in this area as well. The motivation for improving WOLEDs is the need for novel lighting sources that are less expensive and more efficient alternatives to conventional incandescent and fluorescent illumination sources.[2] WOLEDs make attractive candidates as future illumination sources for several reasons, including compact size, the suitability for fabrication on flexible substrates,[3] low operating voltages and good power efficiencies.

Most WOLEDs utilize emission from several different colored emitters, such that the combined output covers the visible spectrum uniformly. While WOLEDs with less than three distinct emitters have been reported, the most common approach in WOLEDs is to use three separate emitters, that is, blue, green and red. It has been demonstrated that three emitters can be mixed together in a single layer to achieve the desired white emission.[4] However, this approach is problematic because energy readily transfers from the higher energy blue dye to the green dye and from the green dye to the red dye. Therefore, careful adjustment of the concentration of each dye is required to achieve a well-balanced emission color. A solution to this energy transfer problem is to segregate the dyes into different layers. Efficient WOLEDs have been prepared using this stacked concept with both fluorescent[5] and phosphorescent emitters.[6] More simplified structures have also been described, which use dual component fluorescent blue and orange emitters doped into separate layers.[5c,7] While stacking the emitters eliminates these energy transfer problems, the device architecture can become significantly more complicated due to difficulties in achieving balanced carrier recombination and exciton localization in each of the separate emitting layers.

† Electronic supplementary information (ESI) available: emission spectra as a function of doping concentration for **3** in CBP, as well as the absorption and emission spectra of Irppz, CBP and mCP. See http://www.rsc.org/suppdata/nj/b2/b204301g/

A further simplification of the device structure can be achieved by using an exciplex as the emitting species. An exciplex is a metastable complex formed by associative excited state interactions between two different molecules. Exciplexes are known to emit over a wide spectral range and have been used in several WOLED architectures.[8–10] Although the use of exciplex emission simplifies the structure of white OLEDs, the efficiency of these devices remains very low, typically no more than 0.6 lm W^{-1}, due to the inherent low luminescence efficiency of the exciplexes described in the literature.[8–10]

Recently, we have reported a new approach to the fabrication of WOLEDs that combines the monomer and excimer phosphorescence of two emitters co-doped into a single emissive layer.[11] This approach has led to a significant simplification of the device structure without a loss in efficiency. Continuing this study, we now report the achievement of well balanced white emission from an emissive layer with only a single luminescent dopant, which emits simultaneously from monomer and aggregate states. Single dopant WOLEDs give voltage independent white emission with external efficiencies as high as 6.4% (ca. 12 lm W^{-1}). In addition to reducing the complexity of the device structure, single dopant WOLEDs may also solve the problems associated with differential dopant aging. WOLEDs utilizing multiple dopants may change color over time, due to differences in the degradation rates of each dopant. It is anticipated that a single dopant WOLED would not suffer from this drawback.

The first section in this paper details the photoluminescent analysis of doped thin films, so as to optimize the emission ratios of the monomer and aggregate states in the emissive layer. It is important to note that doping concentrations of >5 wt % are typically required to efficiently quench the host luminescence and achieve good carrier transport in phosphorescent OLEDs.[12–14] Therefore, one requirement for a single dopant WOLED is to have the proper monomer/aggregate emission ratio for white emission at a high enough doping concentration that will also give a good photon-to-electron quantum efficiency. This optimization was achieved by modifying the steric bulk of the dopant molecule and by changing the host matrix material. Both approaches affected the degree of association of the dopant in the emissive layer and hence the ratio of the emissive states. The second section in this paper demonstrates efficient single dopant WOLEDs. An architecture is used that utilizes a novel electron blocking material, *fac*-tris(1-phenylpyrazole)iridium(III), to confine exciton recombination to the doped luminescent layer. The performance characteristics of these devices are described.

Experimental

Equipment

Absorption spectra were recorded on an AVIV Model 14DS-UV-Vis-IR spectrophotometer (re-engineered Cary 14) and corrected for background due to solvent absorption. Emission spectra (photoluminescence and electroluminescence) were recorded on a PTI QuantaMaster™ Model C-60SE spectrofluorometer, equipped with a 928 PMT detector and corrected for detector response. Phosphorescence lifetime measurements were performed on the same fluorimeter equipped with a microsecond Xe flash lamp and were limited to lifetimes >2 μs. NMR spectra were recorded on Bruker AC 250 MHz or AM 360 MHz instruments. Solid probe MS spectra were taken with a Hewlett Packard GC/MS instrument with electron impact ionization and model 5873 mass selective detector. Elemental analyses were performed by the Microanalysis Laboratory at the University of Illinois, Urbana-Champaign.

Synthesis

Solvents and reagents were purchased form Aldrich Chemical Company. The reagents were of the highest purity available and used as received.

The Pt complexes (**1**–**4**) were prepared by a procedure that is detailed elsewhere.[15] A general description is given here. The ligand 2-(2,4-difluorophenyl)pyridine (F$_2$ppy) was prepared by Suzuki coupling of 2,4-difluorophenylboronic acid and 2-bromopyridine (Aldrich).[16] The Pt(II) μ-dichloro-bridged dimer [(F$_2$ppy)$_2$Pt(μ-Cl)$_2$Pt(F$_2$ppy)$_2$] was prepared by a modified method of Lewis.[17] The dimer was treated with 3 equiv. of the chelating diketone ligand and 10 equiv. of Na$_2$CO$_3$. 2,6-Dimethyl-3,5-heptanedione and 6-methyl-2,4-heptanedione were purchased from TCI. 3-Ethyl-2,4-pentanedione was purchased from Aldrich. The solvent was removed under reduced pressure and the compound purified chromatographically. The product was recrystallized from dichloromethane–methanol and then sublimed. The characterization data (NMR and mass spectra, as well as CHN analysis) for **1** matched those reported.[15] The characterization data for compounds **2**, **3**, and **4** are given below. Based on NMR spectra, compound **4** was determined to be a mixture of 2 isomers in an approximate 1:1 ratio due to the asymmetry of the diketonate ligand.

fac-Ir(ppz)$_3$ was prepared from Ir(acac)$_3$ by a procedure analogous to the one reported for *fac*-Ir(ppy)$_3$.[18] Ir(acac)$_3$ (3.0 g) and 1-phenylpyrazole (3.1 g) were dissolved in 100 ml glycerol and refluxed for 12 h under an inert atmosphere. After cooling the product was isolated by filtration and washed with several portions of distilled water, methanol, ether and hexanes and then vacuum dried. The crude product was then sublimed in a temperature gradient of 220–250 °C to give a pale yellow product (yield 58%)

The synthesis of mCP was based on a known literature procedure using palladium-catalyzed cross coupling of aryl halides and arylamines.[19]

[2-(4′,6′-Difluorophenyl)pyridinato-*N*,*C*$^{2'}$]platinum(II) (2,6-dimethyl-3,5-heptanedionato-*O*,*O*), 2. ^{1}H NMR (250 MHz, CDCl$_3$): ppm 9.01 (d, *J* = 5.8 Hz, 1H), 7.96 (d, *J* = 7.8 Hz, 1H), 7.82 (dd, *J* = 7.5, 6.8 Hz, 1H), 7.13 (m, 2H), 6.56 (ddd, *J* = 12.3, 9.2, 2.7 Hz, 1H), 5.50 (s, 1H), 2.55 (hep, *J* = 7.2 Hz, 1H), 2.54 (hep, *J* = 6.8 Hz, 1H), 1.20 (d, *J* = 6.8 Hz, 6H), 1.19 (d, *J* = 6.8 Hz, 6H). Anal. calcd for C$_{20}$H$_{21}$F$_2$NO$_2$Pt: C 44.45, H 3.92, N 2.59; found: C 44.39, H 3.87, N 2.68.

[2-(4′,6′-Difluorophenyl)pyridinato-*N*,*C*$^{2'}$]platinum(II) (3-ethyl-2,4-pentanedionato-*O*,*O*), 3. ^{1}H NMR (250 MHz, CDCl$_3$): ppm 8.95 (d, *J* = 5.1 Hz, 1H), 7.94 (d, *J* = 8.5 Hz, 1H), 7.80 (dd, *J* = 8.2, 7.2 Hz, 1H), 7.1 (m, 2H), 6.54 (ddd, *J* = 11.9, 9.2, 2.4 Hz, 1H), 2.38 (q, *J* = 6.8 Hz, 2H), 2.14 (s, 3H), 2.13 (s, 3H), 1.07 (t, *J* = 7.5 Hz, 3H). Anal. calcd for C$_{18}$H$_{17}$F$_2$NO$_2$Pt: C 42.19, H 3.34, N 2.73; found: C 42.15, H 3.26, N 2.77.

[2-(4′,6′-Difluorophenyl)pyridinato-*N*,*C*$^{2'}$]platinum(II) (6-methyl-2,4-heptanedionato-*O*,*O*), 4. ^{1}H NMR (250 MHz, CDCl$_3$): ppm 8.98 (two overlapped d, *J* = 5.8 Hz, 1H), 7.95 (d, *J* = 7.8 Hz, 1H), 7.81 (dd, *J* = 7.5, 7.5 Hz, 1H), 7.10 (m, 2H), 6.56 (ddd, *J* = 11.9, 9.2, 2.0 Hz, 1H), 5.45 (s, 1H), 2.14 (s, 2H), 2.12 (m, 1H), 2.00 (two overlapped s, 3H), 0.97, 0.96 (two overlapped d, *J* = 6.5 Hz, 6H). Anal. calcd for C$_{19}$H$_{19}$F$_2$NO$_2$Pt: C 43.35, H 3.64, N 2.66; found: C 43.41, H 3.65, N 2.77.

***fac*-tris(1-Phenylpyrazolato-*N*,*C*$^{2'}$)iridium(III), (Irppz).** ^{1}H NMR (360 MHz, CDCl$_3$): ppm 7.94 (d, *J* = 2.4 Hz, 3H), 7.18 (dd, *J* = 7.8, 1.0 Hz, 3H), 6.97 (d, *J* = 2.0 Hz, 3H), 6.91 (dd, *J* = 7.8, 7.3, 1.5 Hz, 3H), 6.85 (ddd, *J* = 7.8, 1.9,

1.5 Hz, 3H), 6.77 (dd, J = 7.3, 1.5 Hz, 3H), 6.35 (t, J = 2.4 Hz, 3H). Anal. calcd for $C_{27}H_{21}N_6Ir$: C 52.16, H 3.40, N 13.52; found: C 52.04, H 3.39, N 13.52.

3,5-Bis(*N*-carbazolyl)benzene (mCP). ^{1}H NMR (250MHz, $CDCl_3$): ppm 8.16 (d, J = 7.8 Hz, 4H), 7.85 (dd, J = 8.6, 7.5 Hz, 1H), 7.82 (t, J = 1.8 Hz, 1H), 7.70 (ddd, J = 10.1, 7.9, 2.0 Hz, 2H), 7.54 (d, J = 8.4 Hz, 4H), 7.44 (t, J = 7.6 Hz, 4H), 7.31 (t, J = 7.7 Hz, 4H). Anal. calcd for $C_{30}H_{20}N_2$: C 88.21, H 4.93, N 6.86; found: C 88.3, H 4.91, N 7.01.

Estimation of HOMO and LUMO energies

The HOMO energies for NPD, CBP, Irppz, BCP, Alq_3 and mCP were determined by photoelectron spectroscopy, using an AC-1 (Riken Keiki Co., Japan) UV photoelectron spectrometer. The values determined here are consistent with literature values for NPD, CBP, BCP and Alq_3.[20] The LUMO energies were estimated by using the optical energy gap of each material to approximate its carrier gap. The low energy edge of the absorption spectra for Irppz and mCP (370 and 350 nm, respectively) were used as their optical gaps. The HOMO and LUMO values for **1** were taken from the literature.[11]

OLED fabrication

Prior to device fabrication, ITO on glass was patterned as 2 mm wide stripes with a resistivity of 20 $\Omega \square^{-1}$. The substrates were cleaned by sonication in soap solution, rinsed with deionized water, boiled in trichloroethylene, acetone and ethanol for 3–4 min in each solvent and dried with nitrogen. Finally, the substrates were treated with UV ozone for 10 min.

Organic layers were deposited sequentially by thermal evaporation from resistively heated tantalum boats onto the substrate at a rate of 2.5 Å s^{-1}. The base pressure at room temperature was $3–4 \times 10^{-6}$ torr. The rate for single component layers was controlled using one crystal monitor that was located near the substrate. A second crystal monitor located near the evaporation source of the dopant was used to control the rate of dopant molecule incorporation into the host matrix. The additional monitor was screened from the host evaporation, allowing for increased precision of the dopant concentration.

After organic film deposition, the chamber was vented and a shadow mask with a 2 mm wide stripe was put onto the substrate perpendicular to the ITO stripes. A cathode consisting of 10 Å LiF followed by 1000 Å of aluminum was deposited at a rate of 0.3–0.4 Å s^{-1} for LiF and 3–4 Å s^{-1} for aluminum. OLEDs were formed at the 2 × 2 mm squares where the ITO (anode) and Al (cathode) stripes intersected.

The devices were tested in air within 2 h of fabrication. Device current–voltage and light intensity characteristics were measured using the LabVIEW℗ program by National Instruments with a Keithley 2400 SourceMeter/2000 Multimeter coupled to a Newport 1835-C Optical Meter, equipped with a UV-818 Si photocathode. Only light emitting from the front face of the WOLED was collected and used in subsequent efficiency calculations. Electroluminescence spectra were recorded on a PTI QuantaMaster℗ Model C-60SE spectrofluorometer and corrected for detector response.

Results and discussion

Optimizing the emissive layer

The solid state and solution photophysics of luminescent square planar platinum(II) complexes, chelated with aromatic ligands, have been studied in detail.[15, 21–26] In dilute solution, these complexes generally emit as isolated molecules or monomers from a mixed MLCT/[3]LC excited state (MLCT = metal

to ligand charge transfer, LC = ligand centered). However, as the concentration of the Pt complexes in solution is raised, monomer emission decreases and a broad, lower energy emission band is observed. The low energy emission is typically the result of intermolecular stacking interactions, leading to the formation of either excimers or metal-metal bound oligomers. Excimers involve the formation of excited state dimers.[23,25,26] An excimer is only bound in the excited state and rapidly dissociates to two discrete molecules after relaxation to the ground state. In contrast, metal-metal bound oligomers are stable in the ground state, typically involving the formation of weak Pt⋯Pt bonds. Oligomers of this type have been observed both in solution[22,23,26] and in the solid state.[22–24,26,27] The oligomeric structures seen in crystallographic studies can range in length from dimers to continuous chains.[22,23,26–28] Emission from these oligomeric structures is attributed to a $^3[\pi^* \rightarrow d\sigma^*]$ (MMLCT: metal-metal to ligand charge transfer) transition. The emission spectra observed from both excimer and oligomer states are typically broad and unstructured, falling at lower energy than emission from the monomeric species.

Determining the electronic origin for a low energy transition in the solid state for a single compound can often be achieved by correlating the solid state photophysical behavior with the crystal structure. Unfortunately, differentiating between excimer and oligomer excited states in solution or doped thin films is problematic. The oscillator strengths of the MMLCT absorption transitions are typically very low, making them difficult to resolve from the more intense MLCT transitions. The phosphorescent Pt dopants used here may well be involved in both π-π stacking and metal-metal interactions in the doped films, leading to contributions from both excimeric and oligomeric excited states in the emission spectra. For the present study we will not differentiate between excimer and oligomer states, since we do not have conclusive evidence to show if either transition is more important for the dopants examined here. Hereafter the term "aggregate" will be used to describe both excited state (excimer) and ground state (oligomer) aggregated species.

Modifying the Pt dopant. The synthesis and characterization of the (C∧N)Pt(O∧O) dopants used in this study have been described recently.[15] It has been shown that the alteration of the alkyl groups on the β-diketonate ligand (O∧O) does not affect the solution photophysics of the complex. We examined the role that alkyl substituents on the β-diketonate ligand play in controlling the monomer/aggregate emission ratio for two reasons. First, the separation between the square-planar emitting molecules can be adjusted by increasing the degree of steric bulk of the Pt complex. A Pt complex more sterically encumbered than the planar derivative, **1**, should be less prone to form aggregates that are able to electronically interact. Hence, these complexes should require a higher doping concentration to achieve balanced monomer/aggregate emission. Second, larger alkyl groups should increase the "solubility" of the complex, thereby allowing for more uniform dispersal in the host matrix. The series of Pt complexes (**1–4**, Fig. 1) was examined to find the best compound for balanced emission.

Compounds **2 – 4** have greater steric bulk than compound **1**. Complexes **2** and **3** are symmetric, whereas the β-diketonate ligand of **4** is asymmetric. The resulting Pt complex is a mixture of the two inseparable isomers, determined by ^{1}H NMR to be in an approximate 1:1 ratio, only one of which is shown in Fig. 1. The alternate isomer has the β-diketonate ligand reversed (*i.e.*, methyl group *trans* to the pyridyl group). The narrow emission linewidths observed for dilute solutions of **4** indicate that the two isomers have identical excited state energies.
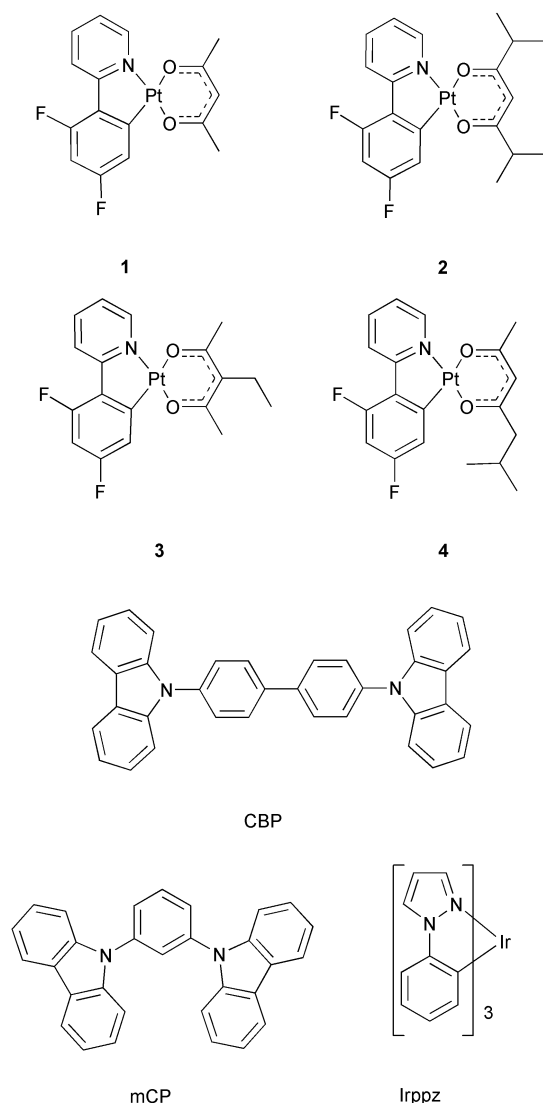
Fig. 1 The structures of the Pt phosphors and OLED materials used in this study.
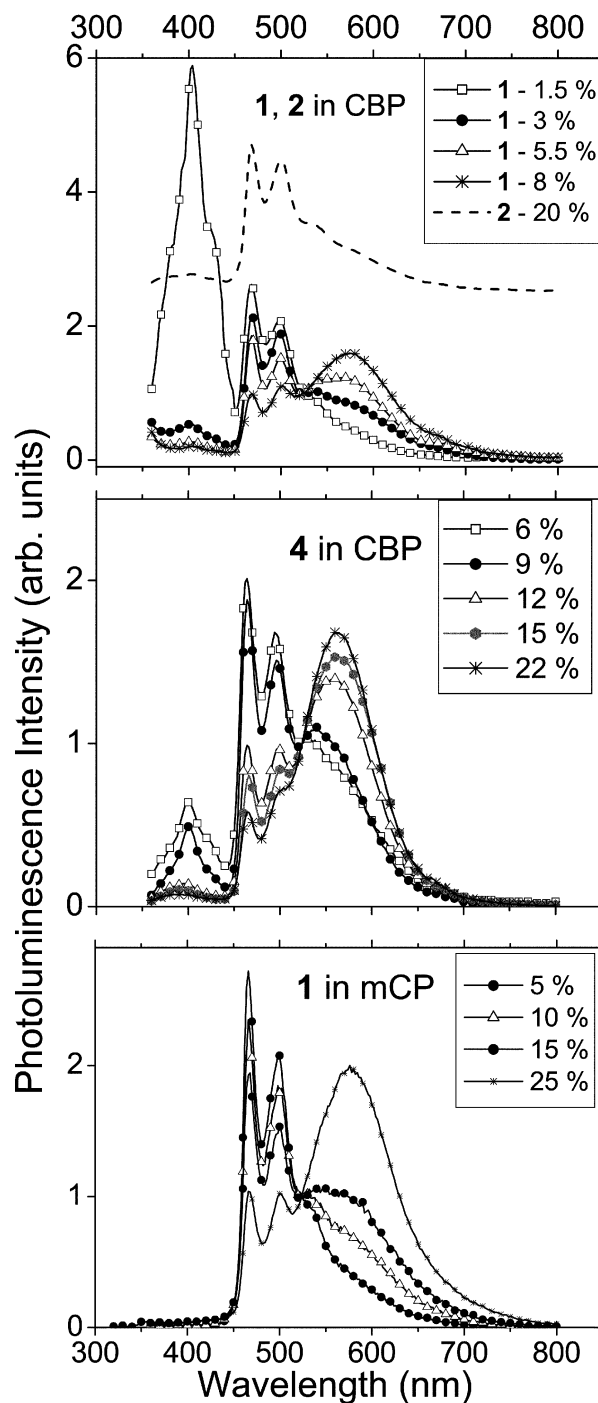

Fig. 2 The photoluminescence spectra for Pt complexes doped into either CBP or mCP thin films are shown. The doping levels for each spectrum are indicated in the legend to each plot. (top): Spectra of **1** and **2** in CBP. The spectrum of **2** doped into CBP at 20% has been vertically shifted for clarity. (middle): Spectra of **4** in CBP. (bottom): Photoluminescence spectra of **1** in mCP and (inset to bottom plot) the CIE coordinate plot for **1** in mCP. The spectra were measured by exciting the film at the excitation maximum of the matrix material (340 nm for CBP and 300 nm for mCP).

Most of our previous work with electrophosphorescent red, yellow, green and blue OLEDs has involved the use of carbazole biphenyl (CBP) as the host material for the doped luminescent layer (Fig. 1).[12–14] CBP has a number of important properties as a matrix material, such as a high triplet energy of 2.56 eV (484 nm)[29] and ambipolar charge transporting properties,[30] that make it an excellent host for phosphorescent dopants. Therefore, it was an obvious choice to begin with in the doping studies described below.

Thin films of CBP doped with 1–30 wt % of Pt complexes **1**–**4** were prepared by co-depositing the two materials onto a glass substrate. The photoluminescent excitation spectra for all of the doped films are identical to the excitation spectra of an undoped CBP film, however, emission comes primarily from the dopant, demonstrating that energy transfer from CBP to dopant is an efficient process at >3 wt % doping levels. The peak positions of the monomer (λ_{max} = 468, 500, and 540 nm) and aggregate ($\lambda_{max} \sim 580$ nm) transitions are the same for all four dopants and do not shift in energy with increasing dopant concentration. The spectra of **1** doped into CBP at a range of different concentrations are shown in Fig. 2. At a 1.5 wt % doping level, emission from **1** is that of the monomer, closely resembling the spectrum observed for **1** in dilute fluid solution. Fluorescence from CBP is also observed (λ_{max} = 406 nm), since this doping level is too low to effectively quench all the CBP emission. As the doping level is

increased, the band at 580 nm grows in, due to the aggregate emission. The aggregate emission ultimately dominates the spectrum at doping levels of 8 wt % and higher. At intermediate doping levels (3–5 wt %), both monomer and aggregate emission are observed from a single doped film. The effect of increasing the size of the alkyl groups can be seen by comparing the spectra of 8 wt % doped **1** to that of 20 wt % doped **2** in CBP. The 8 wt % doped film of **1** shows nearly complete aggregate emission, while the 20 wt % doped film of **2** shows nearly

exclusive monomer emission. Hence, changing the methyl groups in **1** to *i*-propyl groups in **2** strongly suppresses aggregate formation in doped CBP.

In order to achieve balanced monomer/aggregate emission at > 10 wt % doping levels, a molecule is needed that has intermediate steric bulk between that of **1** and **2**. To that end, films of compounds **3** and **4** were examined. At low doping levels of either **3** or **4**, weak CBP fluorescence is observed, as is the case for compounds **1** and **2**. Based on the photoluminescence studies, compound **3** appears to have greater steric bulk than **1**, giving balanced monomer/aggregate emission at ~8 wt % doping levels (see Electronic supplementary information; ESI). The emission spectra of **4** doped CBP shows the expected transition from monomer to aggregate emission as the concentration is increased, however, for this derivative, balanced monomer/aggregate emission is observed at doping levels approaching 10 wt % (Fig. 2). Thus, compound **4** has the appropriate amount of steric bulk to give a balance of monomer and aggregate emission at concentrations necessary for WOLED fabrication and, therefore, was the best dopant option for use with the CBP host matrix material.

Modified host matrices. The second approach taken to vary the monomer/aggregate ratio involved modifying the host matrix material. During the growth of doped films, there are competing processes between the aggregation of dopants and their dispersion in the host matrix. If the host acts as a good solvent, the dopants will be more evenly dispersed in the film, favoring monomeric species. A poorly solvating host matrix will not disperse the monomer dopant efficiently, leading to dopant aggregation. Two different materials (CBP and mCP, Fig. 1) have been examined, which give different degrees of aggregation of **1**.

The spectra of **1** doped in mCP, at a range of concentrations, are shown in Fig. 2. The wavelengths of the emission maxima for the monomer and aggregate states of **1** doped into mCP are the same as those of **1** in CBP. Balanced monomer/aggregate emission is observed at a doping level of approximately 15 wt %, roughly three times the concentration required to achieve an equivalent monomer/aggregate emission ratio from **1** doped CBP films. This suggests that mCP is a better solvent for **1**, leading to fewer **1**···**1** interactions in the doped mCP film, at a given concentration.

In contrast to the CBP doped films, no host emission is observed in the photoluminescence spectra of lightly doped mCP films (< 1 wt % **1**), indicating that energy transfer from mCP to **1** is more efficient than from CBP to **1**. Despite the high triplet energy of CBP (phosphorescence λ_{max} = 460 nm),[29] energy transfer from CBP to blue phosphorescent dopants, such as the Pt complexes used here, is an endothermic process.[11,14] In contrast, mCP has a phosphorescence spectrum peaked at 410 nm[31] (see ESI), making energy transfer from mCP to the Pt complex dopants a more efficient, exothermic process. A more efficient energy transfer from the host to the dopant will affect the amount of dopant necessary to quench emission, as observed.

Both CBP and mCP have low dipole moments (*ca.* 0.5 D), so electrostatic interactions between the dopants and host materials are expected to be similar. This is consistent with the observation that the spectra of monomer and aggregate states for doped mCP and CBP films are the same. Our best explanation for the differences between CBP and mCP, which give rise to differing dopant solubilities, is related to their molecular structures. Planar molecules tend to have high association energies, which promote crystallization and hinder glass formation.[31] CBP is expected to be largely planar in the solid state. This is consistent with our observation that undoped CBP thin films rapidly crystallize when deposited directly on glass or ITO substrates. The high CBP association energy may tend to exclude monomer dopant, leading to aggregate formation at moderate
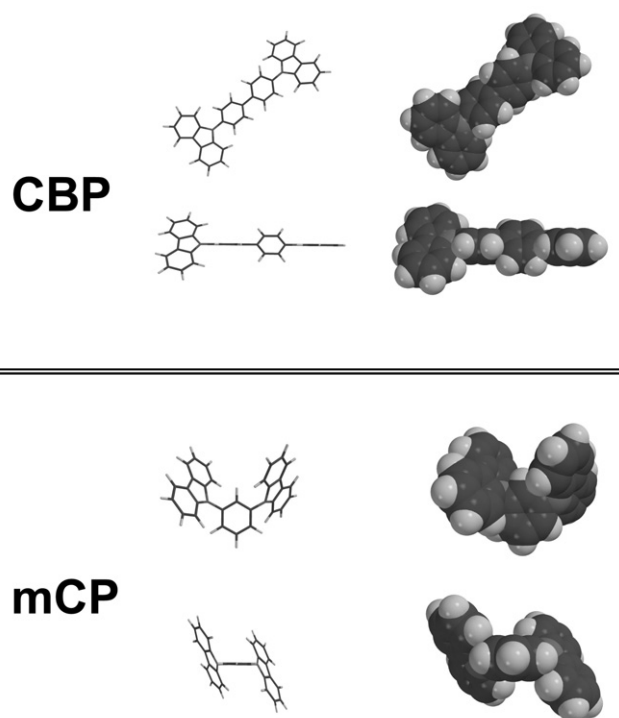

Fig. 3 The energy minimized structures of the CBP and mCP host molecules.[33]

doping levels.[32] mCP readily forms a stable glass when deposited on either inorganic or organic substrates, suggesting it has a nonplanar ground state structure.[31] The glass transition temperature for mCP is 65 °C. Steric interactions between adjacent carbazole groups and the phenyl ring lead to a prediction that both CBP and mCP should have nonplanar ground state structures, as seen in the geometry of the energy minimized structures in Fig. 3.[33] While the minimized structure of CBP appears somewhat nonplanar, it is important to note that the calculated energy difference between the structure shown and the planar conformer is only 18 kJ mol⁻¹. In contrast, the energy cost to planarize mCP is 35 kJ mol⁻¹. The principal cause of the large barrier to flatten mCP is H···H repulsions between adjacent carbazoles, interactions that are absent in CBP. Based on the structural differences, we expect the degree of solvation of a square planar Pt dopant by mCP to be very different from that of CBP. This change significantly affects the monomer/aggregate ratio at a given doping level in CBP *vs.* mCP.

The CIE coordinates and the color rendering index (CRI) for the photoluminescence spectra of **1** doped into mCP are given in Table 1. Concentrations between 4–10 wt % gave the CIE coordinates closest to white (0.33, 0.33) while the maximum CRI was observed for concentrations ranging between

Table 1 CIE coordinates and color rendering indices for photoluminescence spectra of **1** doped mCP films at a range of different dopant concentrations

Concentration/wt %	CIE x	CIE y	CRI
0.1	0.15	0.28	–
0.5	0.19	0.32	–
4.5	0.21	0.35	44.5
10	0.27	0.39	59.7
15	0.32	0.41	68.3
20	0.32	0.39	73.2
25	0.41	0.46	64.1
30	0.41	0.45	69.2

15–20 wt %. At the higher concentrations, the CIE coordinates are close to those found in incandescent lamps (*ca.* 0.41, 0.41). Therefore, the 10–20 wt % concentration range for **1** doped mCP was chosen to be optimal for use in WOLEDs.

Single dopant WOLEDs

OLEDs of the general structure ITO/NPD/CBP:dopant/ BCP/Alq$_3$/LiF/Al [NPD = *N,N'*-diphenyl-*N,N'*-bis(1-naph-thyl)benzidine, BCP = bathocuproine, Alq$_3$ = aluminum tris(8-hyrdroxyquinolate)] have been fabricated previously and have been proven to be very effective for red-to-green phosphorescent OLEDs.[1,6,12,13] The doped CBP luminescent layer is sandwiched between the hole transporting layer (HTL, *i.e.*, NPD) and the hole blocking layer (HBL, *i.e.*, BCP). The HBL is used to confine both carriers and excitons to the luminescent layer, preventing hole and exciton leakage into the electron transporting layer (ETL, *i.e.*, Alq$_3$). OLEDs of the general structure ITO/NPD/CBP:**4**/BCP/Alq$_3$/LiF/Al have been shown to emit white light from a single dopant luminescent layer (*i.e.*, CBP doped with **4**).[11] Unfortunately, while this device gave the desired white emission (CIE = 0.33, 0.31; CRI = 86 at 11 V), the electroluminescence (EL) spectrum had a significant contribution from NPD emission.[11] As the bias was increased, the NPD emission band (λ_{max} = 430 nm) grew relative to the monomer/aggregate features, dominating the EL spectrum at biases of 10 V and above. The cause of this NPD emission was either electron or exciton leakage from the luminescent layer into the NPD layer. This is a problem for these devices, because the dopant is a high energy (blue) phosphorescent emitter. High energy phosphorescent dopants tend to have high energy LUMO levels, approaching those of the transport and host materials.[14] If the dopant LUMO level approaches the LUMO energy of the NPD, electrons can leak into the NPD layer. Likewise, exciton leakage into the HTL layer can occur as the emission energy of the dopant approaches the absorption energy of NPD. The voltage dependent NPD emission in the WOLED described above is indicative of poor charge confinement, which may decrease OLED efficiency. The energy level diagram for this device, shown in Fig. 4, illustrates that the barrier for migration of electrons from the dopant/CBP LUMO levels to the NPD LUMO may be comparable to the hole injection barrier from NPD into the emissive layer. Eliminating electron/exciton leakage into the HTL should improve both the WOLED efficiency and color stability. Therefore, introduction of an electron/exciton blocking layer (EBL) between the HTL and luminescent layer was deemed necessary to improve the device characteristics.

An efficient EBL material needs to fulfill several criteria. It must have a wide energy gap to prevent exciton leakage into the HTL, a high LUMO level to block electrons, and a HOMO level above that of the HTL. We have found that the *fac*-tris(1-phenylpyrazolato-*N,C$^{2'}$*)iridium(III) (Irppz, Fig. 1) complex satisfies these requirements. The Irppz complex emits exclusively from a phosphorescent excited state (λ_{max} = 414 nm at 77 K, τ = 15 μsec). The optical gap for this complex was taken as the low energy edge of the absorption spectrum, at 370 nm (3.4 eV). This estimate of the optical gap represents a lower limit for the carrier gap. Irppz shows a reversible oxidation in fluid solution at 0.38 V (*vs.* ferrocene/ferrocenium), but no reduction wave occurs out to −3.0 V in DMF, consistent with a carrier gap of >3.4 eV. The HOMO energy for Irppz was measured by ultraviolet photoelectron spectroscopy (UPS) and found to be 5.5 eV. Using the Irppz optical gap to approximate the carrier gap, we estimate the Irppz LUMO is 2.1 eV, well above both the CPB and dopant LUMOs. The energy scheme of Fig. 4 suggests that Irppz should make an excellent EBL.
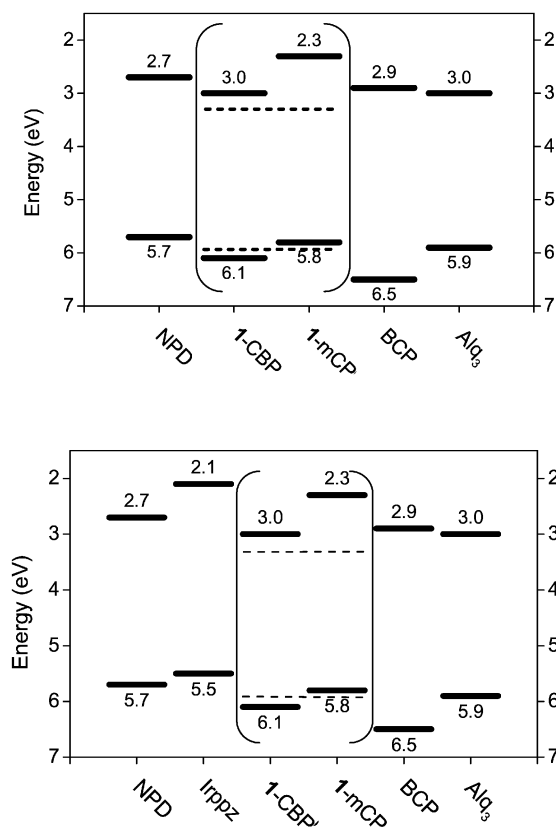

Fig. 4 Energy level diagrams showing the HOMO and LUMO levels for the OLED materials investigated here. The energy for each orbital is listed below (HOMOs) or above (LUMOs) the appropriate bar. The HOMO and LUMO levels for the emissive dopant **1** is shown as a dashed line in each of the plots. The doped luminescent layers (CBP or mCP) are enclosed in brackets. Each device had either a CBP or an mCP layer, not both. The top plot shows the diagram for a four-layer OLED (no electron blocking layer), and the bottom plot shows a similar OLED with an Irppz EBL.

The spectra and CIE coordinates (inset) of a single dopant WOLEDs (using 8, 10 and 12 wt % **4** in CBP), with an Irppz EBL, are shown in Fig. 5. The devices give an EL spectrum consistent with only dopant emission, that is no NPD emission is observed at any bias level. The ratio of monomer/aggregate contributions in the EL spectrum is also invariant with applied bias, leading to a voltage independent, high quality white emission (0.36, 0.44 and CRI of 67 for the 10% doped device). The peak brightness of the 10% doped device was 8000 cd m^{-2} and the maximum quantum efficiency was $3.3 \pm 0.3\%$ (7.3 ± 0.7 lm W^{-1}) at 0.5 cd m^{-2}, dropping to $2.3 \pm 0.2\%$ (5.2 ± 0.3 lm W^{-1}) at 500 cd m^{-2}. The quantum efficiency of the device with an Irppz blocking layer is nearly double that of the device with no EBL (peak efficiency = 1.9%).[11] It is also apparent from the current–voltage and quantum efficiency plots that increasing the dopant concentration improves the performance of the devices (higher quantum efficiency and lower leakage current at a given bias). However, the higher doping levels also increase the amount of aggregate emission in the spectrum, leading to a shift in the color of the device from white to yellow.

The use of the mCP host in place of CBP significantly improves the device performance. A device was fabricated with the structure NPD (400 Å)/Irppz (200 Å)/mCP : **1** (16%, 300 Å)/BCP (150 Å)/Alq3 (200 Å)/LiF (10 Å)/Al (1000 Å). The efficiency, current–voltage characteristics, and spectra of the device are shown in Fig. 6. The higher doping concentrations and improved energy transfer from mCP to the dopant gave a maximum quantum efficiency of $6.4 \pm 0.6\%$ (12.2 ± 1.4 lm
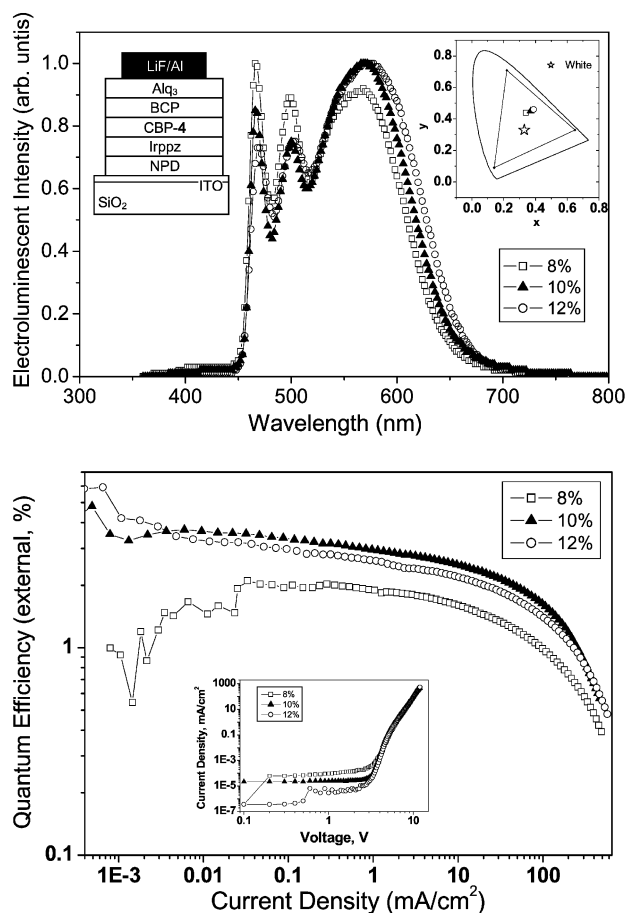
Fig. 5 WOLED device properties for devices with an Irppz EBL [ITO/NPD (400 Å)/Irppz (200 Å)/CBP:**4** (300 Å)/BCP (150 Å)/Alq$_3$ (200 Å)/ LiF–Al]. A schematic drawing of the device is shown as an inset to the top plot. Data for devices doped at 8, 10, 12% are shown. The spectra and CIE coordinates (inset) are shown in the top plot and the quantum efficiency *vs.* current density and current–voltage characteristics (inset) are shown in the bottom plot.

W^{-1}, 17.0 cd A^{-1}) at low brightness levels (1 cd m^{-2}) and 4.3 ± 0.5% (8.1 ± 0.6 lm W^{-1}, 11.3 cd A^{-1}) at 500 cd m^{-2}. The quantum efficiencies demonstrated by these mCP·**1** WOLEDs are the highest reported efficiencies for a WOLED.[4–11] The quantum efficiency decreases with increasing current density, as observed for other devices,[34] however, the decrease is less severe than in most other electrophosphorescent devices. If the Irppz EBL is omitted (*i.e.*, NPD/mCP-**1**/BCP/Alq$_3$), the EL spectrum again has a significant contribution from NPD and quantum efficiency of the devices drops by roughly a factor of two (see Fig. 6). Overall, the Irppz EBL increases the OLED efficiency, removes NPD emission from the spectra and makes the spectrum independent of voltage.

The high color rendering index of a single dopant OLED is demonstrated in Fig. 7. The OLEDs used for this figure are a mCP:**1** based device. The CIE diagram is illuminated *only* by the mCP·**1** OLEDs. All of the colors on the diagram are readily distinguished. The spectral characteristics of these single dopant WOLEDs clearly make them suitable for use as white light illumination sources.

Conclusion

We have demonstrated the most efficient WOLEDs reported.[4–11] These devices emit from a single doped luminescent layer, containing only one emissive dopant. In order to accomplish
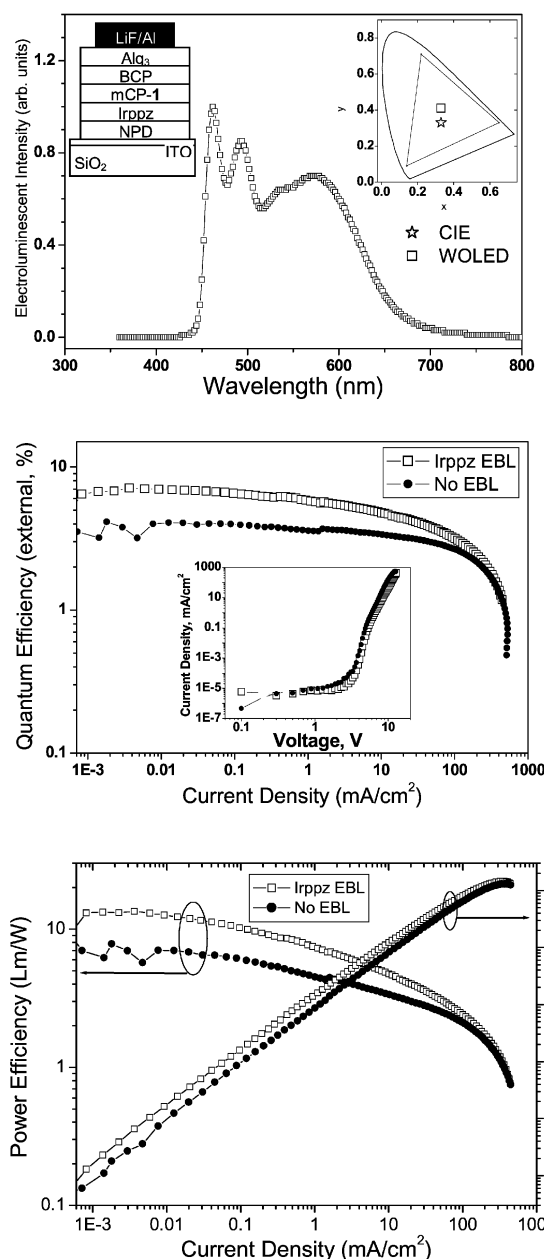

Fig. 6 WOLED device properties for a mCP based WOLED [ITO/NPD (400 Å)/Irppz (200 Å)/mCP:**1** (doping level 16%, 300 Å)/BCP (150 Å)/Alq$_3$ (200 Å)/ LiF–Al]. A schematic drawing of the device with the Irppz EBL is shown as an inset to the top plot. The spectra and CIE coordinates (inset) are shown in the top plot and the quantum efficiency *vs.* current density and current–voltage characteristics (inset) are shown in the middle plot. Lumens per watt and brightness *vs.* current density plots for the WOLED and the related structure without the Irppz EBL are shown in the bottom plot.

this it was important to control both the emission character, by tuning the degree of dopant-dopant and dopant-host interactions, and the carrier/exciton confinement in the device. The structure reported here utilizes an electron blocking layer (Irppz) to confine carriers and excitons to the desired luminescent layer. This structure may be useful for monochromatic electrophosphorescent OLEDs as well as for WOLEDs. As the dopant energies are increased toward the blue end of the spectrum, the dopant energy gap can exceed that of the available transport and host materials, leading to poor confinement of charge and energy in the desired luminescent layer. The approach developed here to eliminate HTL (NPD) emission and improve the quantum efficiency may work equally well
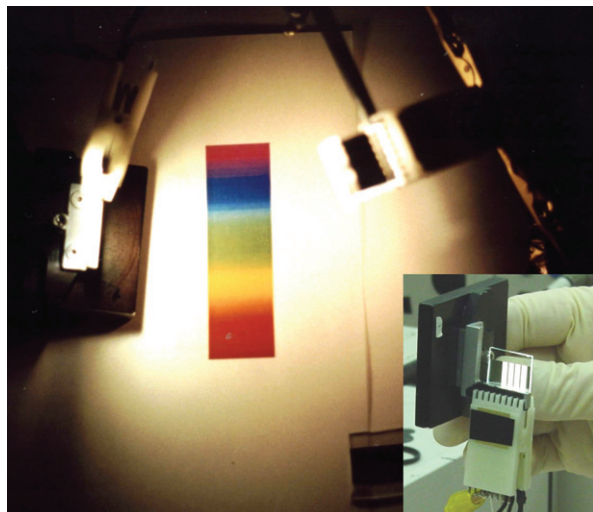
Fig. 7 A color bar illuminated only by the singly doped white OLED described in Fig. 6. A picture of the WOLEDs in room light is shown to the lower left.

for blue electrophosphorescent OLEDs, by effectively controlling the recombination and emission zones of the device. Studies in this area are ongoing.

The use of only a single dopant in WOLEDs significantly simplifies the fabrication of WOLEDs relative to other approaches to white organic electroluminescence. It may also solve the problems associated with differential dopant aging. The lifetimes of monochromatic OLEDs, prepared with different dopants, vary over a wide range, due to different chemical and electrochemical stabilities of the various dopants and host materials that are used. While there have been no reports of the lifetimes or color stabilities of WOLEDs, it is expected that WOLEDs utilizing multiple dopants will show different characteristic aging times for each of the dopants. Differential aging of the dopants would change the color of the WOLED over time, as the dopant emission ratio changes. It is expected that a single dopant WOLED will not suffer from these limitations, since the two emission bands (monomer and aggregate) come from the same dopant. Experiments are currently underway with the single dopant WOLEDs reported here to examine their lifetimes and verify that they are color stable over the life of the WOLED.

Acknowledgements

References

1   (a) C. Adachi, M. A. Baldo, S. R. Forrest and M. E. Thompson, *J. Appl. Phys.*, 2001, **90**, 4058; (b) M. Ikai, S. Tokito, Y. Sakamoto, T. Suzuki and Y. Taga, *Appl. Phys. Lett.*, 2001, **79**, 156–158.
2   T. Justel, H. Nikol and C. Ronda, *Angew. Chem., Int. Ed.*, 1998, **37**, 3084–3113.
3   J. Mahon, J. Brown, T. Zhou, P. Burrows and S. Forrest, *Annu. Tech. Conf. Proc. - Soc. Vac. Coaters*, 1999, **42**, 456–459.
4   (a) J. Kido, H. Shionoya and K. Nagai, *Appl. Phys. Lett.*, 1995, **67**, 2281–2283; (b) S. Tasch, E. J. W. List, O. Ekström, W. Graupner, G. Leising, P. Schlichting, U. Rohr, Y. Geerts, U. Scherf and K. Müllen, *Appl. Phys. Lett.*, 1997, **71**, 2883–2885; (c) Y. Kawamura, S. Yanagida and S. R. Forrest, *J. Appl. Phys.*, 2002, **92**, 87–93.
5   (a) Y. S. Huang, J. H. Jou, W. K. Weng and J. M. Liu, *Appl. Phys. Lett.*, 2002, **80**, 2782–2784; (b) C. Ko and Y. Tao, *Appl. Phys. Lett.*, 2001, **79**, 4234–4236; (c) X. Jiang, Z. Zhang, W. Zhao, W. Zhu, B. Zhang and S. Xu, *J. Phys. D: Appl. Phys.*, 2000, **33**, 473–476; (d) S. Liu, J. Huang, Z. Xie, Y. Wang and B. Chen, *Thin Solid Films*, 2000, **363**, 294; (e) J. Kido, M. Kimura and K. Nagai, *Science*, 1995, **267**, 1332–1334.
6   B. D'Andrade, M. Thompson and S. Forrest, *Adv. Mater.*, 2002, **14**, 147–151.
7   J. Yang, Y. Jin, P. Heremans, R. Hoefnagels, P. Dieltiens, F. Blockhuys, H. Geise, M. Van der Auweraer and G. Borghs, *Chem. Phys. Lett.*, 2000, **325**, 251–256.
8   J. Thompson, R. Blyth, M. Mazzeo, M. Ani, G. Gigli and R. Cingolani, *Appl. Phys. Lett.*, 2001, **79**, 560–562.
9   C.-I. Chao and S.-A. Chen, *Appl. Phys. Lett.*, 1998, **73**, 426–428.
10 J. Feng, F. Li, W. Gao and S. Liu, *Appl. Phys. Lett.*, 2001, **78**, 3947–3949.
11 B. D'Andrade, J. Brooks, V. Adamovich, M. E. Thompson and S. R. Forrest, *Adv. Mater.*, 2002, **14**, 1032–1036.
12 D. O'Brien, M. Baldo, M. E. Thompson and S. R. Forrest, *Appl. Phys. Lett.*, 1999, **74**, 442–444.
13 S. Lamansky, P. Djurovich, D. Murphy, F. Abdel-Razzaq, H.-E. Lee, C. Adachi, P. E. Burrows, S. R. Forrest and M. E. Thompson, *J. Am. Chem. Soc.*, 2001, **123**, 4304–4312.
14 C. Adachi, R. Kwong, P. Djurovich, V. Adamovich, M. Baldo, Mark E. Thomson and S. R. Forrest, *Appl. Phys. Lett.*, 2001, **79**, 2082–2084.
15 J. Brooks, Y. Babayan, S. Lamansky, P. I. Djurovich, I. Tsyba, R. Bau and M. E. Thompson, *Inorg. Chem.*, 2002, **41**, 3055–3066.
16 O. Lohse, P. Thevenin and E. Waldvogel, *Synlett*, 1999, **1**, 45–48.
17 B. N. Cockburn, D. V. Howe, T. Keating, B. F. G. Johnson and J. Lewis, *J. Chem. Soc., Dalton Trans.*, 1973, 404–410.
18 K. Dedeian, P. I. Djurovich, F. O. Garces, G. Carlson and R. J. Watts, *Inorg. Chem.*, 1991, **30**, 1685–1687.
19 T. Yamamoto, M. Nishiyama and Y. Koie, *Tetrahedron Lett.*, 1998, **39**, 2367–2370.
20 (a) H. Ishii, K. Sugiyama, E. Ito and K. Seki, *Adv. Mater.*, 1999, **11**, 605–625; (b) I. Hill and A. Kahn, *J. Appl. Phys.*, 1998, **84**, 5583
21 (a) V. M. Miskowski and V. M. Houlding, *Inorg. Chem.*, 1989, **28**, 1529–1533; (b) V. H. Houlding and V. M. Miskowski, *Coord. Chem. Rev.*, 1991, **111**, 145–152; (c) V. M. Miskowski and V. H. Houlding, *Inorg. Chem.*, 1991, **30**, 4446–4452; (d) V. M. Miskowski, V. M. Houlding, C.-M. Che and Y. Wang, *Inorg. Chem.*, 1993, **32**, 2518–2524.
22 J. A. Bailey, M. G. Hill, R. E. Marsh, V. M. Miskowski, W. P. Schaefer and H. B. Gray, *Inorg. Chem.*, 1995, **34**, 4591–4599.
23 T.-C. Cheung, K.-K. Cheung, S.-M. Peng and C.-M. Che, *J. Chem. Soc., Dalton Trans.*, 1996, 1645–1651.
24 G. Y. Zheng and D. P. Rillema, *Inorg. Chem.*, 1998, **37**, 1392–1397.
25 (a) S.-W. Lai, M. C. W. Chan, K.-K. Cheung, S.-M. Peng and C.-M. Che, *Organometallics*, 1999, **18**, 3991–3997; (b) S.-W. Lai, M. C. W. Chan, K.-K. Cheung and C.-M. Che, *Inorg. Chem.*, 1999, **38**, 4262–4267; (c) W. Lu, M. C. W. Chan, K.-K. Cheung and C.-M. Che, *Organometallics*, 2001, **20**, 2477–2486.
26 (a) R. Büchner, C. T. Cunningham, J. S. Field, R. J. Haines, D. R. McMillan and G. C. Summerton, *J. Chem. Soc., Dalton Trans.*, 1999, 711–717; (b) W. Lu, N. Zhu and C.-M. Che, *Chem. Commun.*, 2002, 900–901; (c) S. W. Lai, H. W. Lam, W. Lu, K. K. Cheung and C. M. Che, *Organometallics.*, 2002, **21**, 226–234.
27 J. P. H. Charmant, J. Forniés, J. Gómez, E. Lalinde, R. I. Merino, M. T. Moreno and A. G. Orpen, *Organometallics*, 1999, **18**, 3353–3358.
28 W. B. Connick, R. E. Marsh, W. P. Schaefer and H. B. Gray, *Inorg. Chem.*, 1997, **36**, 913–922.
29 M. A. Baldo and S. R. Forrest, *Phys. Rev. B*, 2000, **62**, 10 958–10 966.
30 C. Adachi, R. Kwong and S. R. Forrest, *Org. Electron.*, 2001, **2**, 37–43.
31 K. Naito and A. Miura, *J. Phys. Chem.*, 1993, **97**, 6240.
32 "Aggregate formation" in this context could mean either the formation of Pt–Pt bonded oligomers or the formation of regions of the film with a high local concentration of dopant that will readily form excimers on excitation.
33 The molecular modeling and energy minimization was carried out at PM3 level using the MacSpartan Pro v. 1.02 software package, Wavefunction Inc, Irvine, CA 92612.
34 M. A. Baldo and S. R. Forrest, *Phys. Rev. B*, 2000, **62**, 10 958–10 966.